Asian Journal of Surgery (2019) 42, 814—822

Available online at www.sciencedirect.com

ScienceDirect

journal homepage: www.e-asianjournalsurgery.com

ORIGINAL ARTICLE

# Analysis of Endonasal Endoscopic Transsphenoidal (EET) surgery pathway and workspace for path guiding robot design

Suwiphat Chalongwongse [a], Sorayouth Chumnanvej [b], Jackrit Suthakorn [a,*]

[a] Center for Biomedical and Robotics Technology (BART LAB), Department of Biomedical Engineering, Faculty of Engineering, Mahidol University, Salaya, Thailand
[b] Neurosurgery Division, Department of Surgery, Faculty of Medicine, Ramathibodi Hospital, Mahidol University, Bangkok, Thailand

Received 7 September 2018; received in revised form 12 December 2018; accepted 25 December 2018
Available online 30 January 2019

**KEYWORDS**
Endoscopic Endonasal Transphenoid (EET);
Medical robotics;
Minimally invasive surgery;
Natural orifice transluminal surgery;
Neurosurgical robots;
Pituitary adenoma;
Robotic surgery

**Summary** *Background:* Endoscopic Endonasal Transsphenoidal Surgery (EETS) is the standard method to treat pituitary adenoma, tumor in the pituitary gland which would affect human beings in terms of hormonal malfunction and other symptoms. This procedure provides extra minimal invasive access in severe cases. The objective of this paper is to design and develop a prototype of EET robot with navigation guidance system based on the study of EET workspace and pathway to determine a safe space for surgical tool insertion.
*Methods:* The EET workspace and its pathway were studied via data collected from EET experiments on 70 cadavers. An optical tracking system was used to detect and record the movement of the surgical tools during the experiments. Delaunay triangulation and Voronoi diagram were utilized to determine the cloud position of the gathered data for EET workspace. Moreover, in order to determine the EET pathway voxelization methods were incorporated.
*Results:* The average diameter of the workspace calculated was 19.08 with 3.32 S. D, the average length and volume of the workspace were 53.9 mm and 15.9cm3, respectively. The S.D values determined for length and volume were 7.2 and 6.02, respectively. For the pathway, a high density area was determined via data obtained through cloud position.
*Conclusion:* Dimension of the EET workspace and characters of EET pathway determine robot's requirements to design and develop EET robotic system. This article demonstrates the conceptual design of an EET robot and successfully accomplishes the goal of guidance and aids in assisting the EET procedures.

* Corresponding author. Fax: +662 441 4254.
*E-mail addresses:* suwiphat.ch@gmail.com (S. Chalongwongse), sorayouth.chu@mahidol.ac.th (S. Chumnanvej), jackrit@bartlab.org, jackrit.sut@mahidol.ac.th (J. Suthakorn).

https://doi.org/10.1016/j.asjsur.2018.12.016

## 1. Introduction

According to the American Board of Neurological Surgery (ABNS), neurosurgery is an integral part of a medical discipline and surgical specialty of the central nervous system, the peripheral nervous system, and the autonomic nervous system that provides care to adult and pediatric patients. This discipline provides treatment for pain or pathological processes and is involved in modifying the function or activity of the nervous system, supporting structures of these systems and their vascular supply.

### 1.1. Endonasal Endoscopic Transsphenoidal surgery

Pituitary Adenoma is a slow-growing tumor in the pituitary gland that regulates essential body hormones as shown in Fig. 1. However, when the tumor cells grow irregularly, they secrete excessive hormones and cause many endocrine diseases. The related symptoms caused by the tumor enlargement are: headache and vision loss. To treat the tumor, there are essentially three methods: drug therapy, radiotherapy and surgery. The direct approach to the tumor, nowadays, is possible through a new technique-Endonasal Endoscopic Transsphenoidal (EET) Surgery.[1–3] EET in the pituitary surgery, follows Natural Orifices Transluminal Endoscopic Surgery (NOTES)[4,5] and operates via nasal cavity through sphenoid sinus. In EET procedure,[3,6–8] a sinus surgical tool is inserted together with the endoscope through the nasal cavity. Hence, enlarges and passes through the sinus openings before removing the tumor. According to growth of surgical methods, several specific surgeries were developed base on EET procedure,[9] such as Arachnoid cyst, pituitary apoplexy and pituitary tumor. Surgical indication of this article is a surgery for pituitary tumor on Sella turcica.

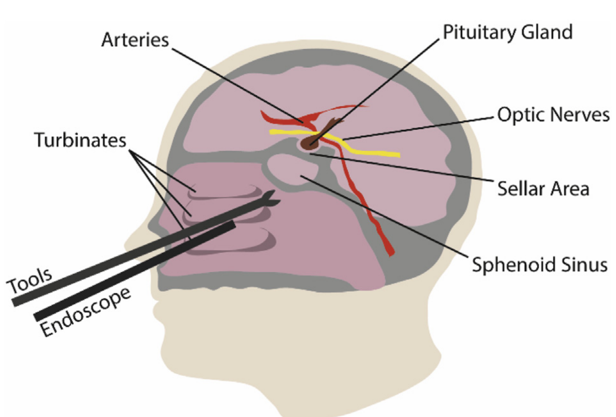


**Figure 1** Pituitary gland on head anatomy.

The EET procedure is still a new technique and only an expert surgeon can perform it. It involves two complicated processes that it requires high level of experienced surgeon. The first one is sphenoid sinus approaching process that lacks anatomical landmark inside nasal cavity. In addition to this, the average operation time is more than 1 h to finish this process. Furthermore, in this procedure nasal mucosa also gets damaged. The second is tumor elimination process, requires precise and accurate movement of surgical tool. This process is operated inside brain area that is surrounded by brain tissue. The EET surgery to remove the tumor takes approximately 2–4 h. Study of EET procedures depict that (26.9%) patients go through post-operative complications. Major postoperative complications are: endocrine system (17.9%), intrasellar complication (2.6%) and nasal or rhinological complication (1.9%).[10–12]

In order to overcome the deficiencies associated with conventional EET, this study is providing a solution in terms of time reduction, precision and accuracy required to reach the target. This robot based system will reduce the time span in a way that the primary pathway i.e. from nasal cavity to sphenoid sinus, to get to the pituitary tumor will be performed by the surgeon, who would be assisted by the robot. The robot will provide assistance in terms of a robot guided receptacle that will direct the accurate pathway for the surgical tool and the endoscope to reach the target. As this procedure involves immense precision to hit the right target, a small deviation or deflection in the pathway may damage the nasal cavity. The EET is a long time consuming procedure as discussed earlier, there are chances of human error in terms of maintaining a stable trajectory throughout the procedure. Therefore, a robot guided receptacle will extract information via fluoroscopic images transferred to the software to set and align its pathway for the surgeon to conduct the surgery smoothly and efficiently. In addition to this with the aid of Fluoroscopy the trajectory of the pathway can be monitored and the images can be obtained via connected computer systems. Thus, this conceptual framework will open new arenas for surgical procedures in the near future. This robot based EET system will operate under the observation of surgeon thus reducing the risk factors associated with a non-guided machine.

## 2. Materials and methods

This research focuses on the study of workspace and pathway of EET surgical procedure. The study performs EET experiments on soft cadavers based on the EET procedure. Soft cadaver is only Thai people that preserved under 0 °C without formalin. Movements of surgical tool are collected during the operations. The collected data is then analyzed for shape, size of EET workspace and the movement of surgical tool during the operation. Purpose of this paper is to design the EET robot based system on the principles of workspace and pathway. Through this system operating time and damage to nasal mucosa would be minimized, in other word.

### 2.1. Analyzation of the EET workspace and EET pathway

In this chapter, EET pathways are analyzed via cloud positions. Voxelization and probability density function are applied to the pathway analyzation. EET workspace is measured via shape, dimension and volume of cloud position. The dimensions of the EET workspace are calculated from the maximum boundary and length of the workspace; determining the distance between the entry points of the nostril to sphenoid sinus. The volume of the workspace is also computed via the cloud position by Delaunay triangulation and Voronoi diagram methods.[13]

#### 2.1.1. Voxelization method on cloud positions

A voxel signifies a value on a regular grid in three-dimensional space. Voxelization method applied to EET workspace is shown in Fig. 2. EET surgical pathway defines and determines the position and orientation of the surgical tool tip at different levels of insertion depth. The overall system transformation matrix is calculated by using a set of points from normalized Cloud positions and rigid transformation techniques.

#### 2.1.2. Probability density function of positions and orientations

EET workspace is based on the voxelization method and is divided into a small cube. The voxels are overlying on cloud positions. Each point is correlated with the position of a voxel. Each voxel consists of several numbers of points as shown in Fig. 2. The number of points on each voxel characterizes the density of the voxel on the EET workspace. High-density values of the voxel signify the position of surgical tool tip and the high frequency used or generally called workspace density function.[14] Probability density function (PDF) method is used to define a high probability position of the surgical tool tip, in addition to voxels with high PDF value. Moreover, the orientation of a surgical tool is also determined by the PDF method. Orientations of each voxel are considered and applied on the orientation of points in voxel by PDF method.

### 2.2. Conceptual design for EET surgical guided robot

#### 2.2.1. Significances of surgical robot on EET procedure

Recently, the endonasal surgery has not yet been demonstrated in a setting of the robotic platform because traditional surgical robots are not well suited to trans nasal surgeries. Traditional surgical robots have large tool diameters and the problem of coordinating multiple tools in the narrow area such as nasal cavities becomes an uphill task. Fluoroscopic images including pre-operation and intra-operation are accomplished. The patient safety is paramount; a robotic platform for EET procedure has advantages to reduce technical barriers and to deliver the benefits of surgical technique to approach sphenoid sinus in patients. EET guided robot is designed to guide/assist surgeon to perform pituitary tumor removing process, especially the tumor on Sella turcica. The robot provides single time insertion for sphenoid sinus followed by instructions from the surgeon.

#### 2.2.2. Conceptual design of EET guiding robot

The conceptual design of an EET surgical assisted robotic system is based on the knowledge of the CIS (Computer Integrated Surgery).[15–17] The EET robot is designed to collaborate with pre-operation and intra-operation on the basis of the CIS concept. During the first step on pre-operation, surgical path planning is determined on 3D reconstructed model from patient CT-scan image. The surgical path is a straight line from entry point of nostril to anterior sphenoid bone.

For intra-operation, the robot is manual placed over the patient's head for initial position setup as shown in Fig. 3.

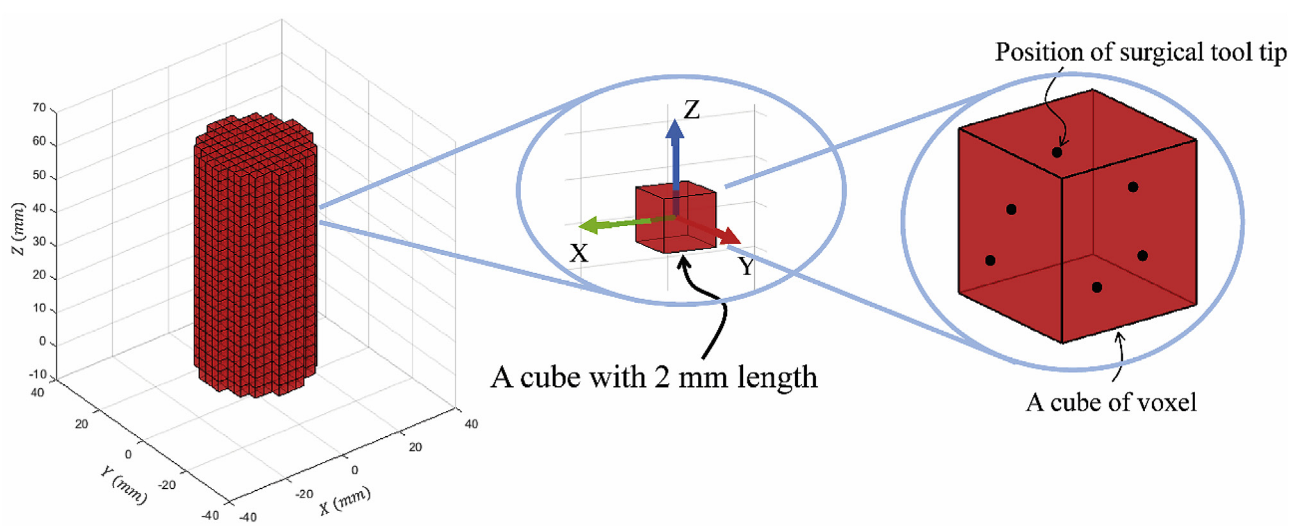


**Figure 2** Voxelization method of EET cloud position.

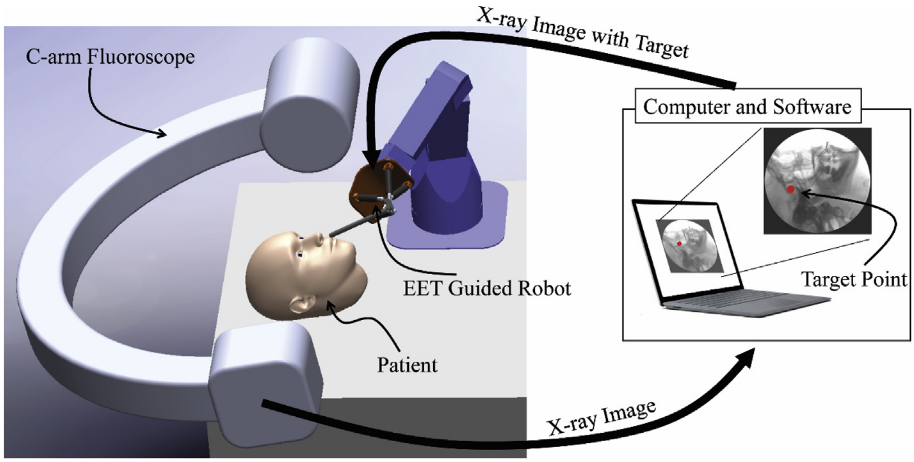


**Figure 3** Conceptual design of EET guided robotic system with robot diagram.

Robot guided EET is connected with fluoroscopy and is set up on the patient. The fluoroscope was used to register the robot, patient and planned path together with image registration method. Then, the robot will automatically align itself in accordance with the planned path. Automatic mechanism is 4 DOFs parallel robot, 2 DOFs for translations and 2 DOFs for rotations. Thereafter, surgeon performs traditional EET surgery through guided tube of the robot to remove tumor.

The surgical tool is attached to the end effector of the automatic mechanism and the auto mechanism is attached to the end effector of the manual mechanism. Position and direction of the surgical tool course are set up at the entry point of nostril by the surgeon. The surgeon manually adjusts the position and direction of the surgical tool. After that, image registration methods are used to map the EET robot with the planned path. The auto mechanism precisely adjusts the position and orientation of the surgical tool according to the planned path as illustrated in Fig. 4a).

The mechanical operation of the automatic mechanism is cooperative with the surgical path planning. The EET guided robot and patients are characterized on the same coordinate by image registration method and the system defines the position and orientation of the robot and planned path. A linear equation of planned path ($r(t)$) is defined from the entry point of nostril ($P_2$) and sphenoid sinus ($P_1$) and where the intersection point between the planned path ($r(t)$) and 2D-plane workspace of robot is estimated by using mathematical method as illustrated in Fig. 4b) and explained in equation (1), where $t$ is a variable parameter.

$$r(t) = (x_1 + (x_2 - x_1)t,\ y_1 + (y_2 - y_1)t,\ z_1 + (z_2 - z_1)t) \qquad (1)$$

From Fig. 4b) an intersect point is calculated with respect to equations (1) and 2D plane-workspace of the guiding robot with the normal vector ($\vec{n}$).

The robotic system drives the tip of the guiding tube to the intersection point position and the orientation of the guiding tube is adjusted to concentricity with the planned path. Alternately robotic system checks the error between the tip of the guiding tube and the intersection point upon the tolerance level and it identifies that the errors are greater than tolerance. The robot repeats the operation again.

## 2.3. Design and development of EET guided robot

### 2.3.1. Robot mechanism

Normally, 2 DOF translations and 2 DOF rotations are required for a guided robot with parallel mechanism due to a small workspace, high payload and especially high precision and accuracy. Planar parallel mechanism and spherical parallel mechanism are realistic to the guided robot with 2-UPS planar parallel mechanism provide 2 DOF translations and 2-UPU spherical parallel mechanism provides 2 DOF rotations.[18] Both the planar parallel mechanism

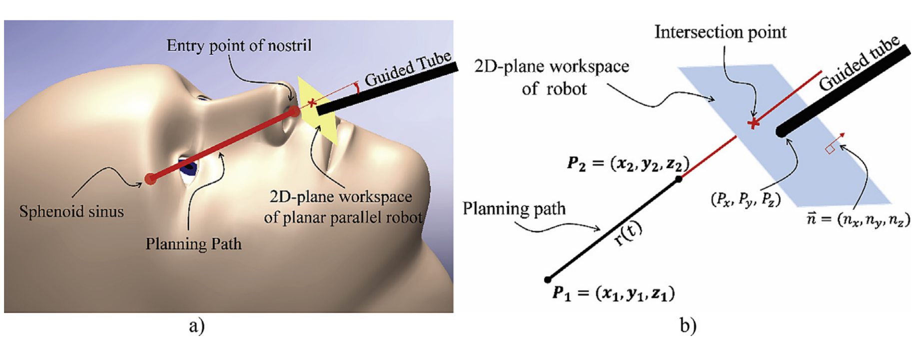


**Figure 4** a) Automatic operation of guiding robot and b) Mathematical diagram of automatic operation.

and spherical parallel mechanism are cooperatively applied on the EET guided robot. Planar parallel mechanism and spherical parallel mechanism are connected together at the end of the effector point as illustrated in Fig. 5. The position of the end effector can be controlled by a planar parallel mechanism and orientation of the end effector can be controlled by a spherical parallel mechanism.

### 2.3.2. Kinematic analysis

In this section kinematic models for the EET, guided robot is explained in detail. Position and orientation of the end effector point are separated from the planar parallel mechanism and spherical parallel mechanism, respectively as shown in Fig. 5. The parameters used in Fig. 5 and in equation (2) are described as follows.

$(X, Y, Z)$ position of end effector point; $(X_{m_i}, Y_{m_i}, Z_{m_i})$ position of joints between fixed base and linear actuator number $i$ on X, Y and Z axis; $P_i$ position of the joints between moving plate and linear actuator number $i$; $l_i$ length of linear actuator number $i$; $A$ *and* $B$ dimensions of the moving plate.

## 2.4. Planar parallel/spherical parallel mechanism

The kinematic model of the planar parallel mechanism and a spherical parallel mechanism is the relationship between 2 linear actuators used and is derived from the geometric solution method[19–22] and algebraic solution method.[23,24] Equation (2) shows the derived inverse kinematic model for the planar parallel mechanism, and the desired position of end effector point with the condition $l_i$ must be greater than $l_{min}$ and less than $l_{max}$. Equation (3) represents the kinematic model $P_i$ which is calculated from the desired orientation of $\varphi_x$ and $\varphi_y$.

$$l_i = \begin{cases} \sqrt{(Y_{m_i} - Y)^2 + (X_{m_i} - X)^2}, & \mathit{if}\ \ l_{min} < \sqrt{(X - X_{m_i})^2 + (Y - Y_{m_i})^2} < l_{max} \\ \mathit{Invalid}, & \mathit{Otherwise} \end{cases} \tag{2}$$

$$P_i = \left( \left( Rot_y(\varphi_y) \cdot Rot_x(\varphi_x) \right) \cdot \left( \frac{B}{2}, A, 0 \right)^T \right) + (X, Y, Z)^T \tag{3}$$

Where $Rot_y(\varphi_y)$ and $Rot_x(\varphi_x)$ is the rotation matrix of angle $\varphi_y$ and $\varphi_x$ around X-axis and Y-axis, respectively.

$$l_i = \begin{cases} \left\| P_i - (X_{m_i}, Y_{m_i}, Z_{m_i}) \right\|, & \mathit{if}\ \ l_{min} < \left\| P_i - (X_{m_i}, Y_{m_i}, Z_{m_i}) \right\| < l_{max} \\ \mathit{Invalid}, & \mathit{Otherwise} \end{cases} \tag{4}$$

Equation (4) represents the length of linear actuators from the desired orientation of end effector point and which is obtained from substituting $P_i$ to the above equation.

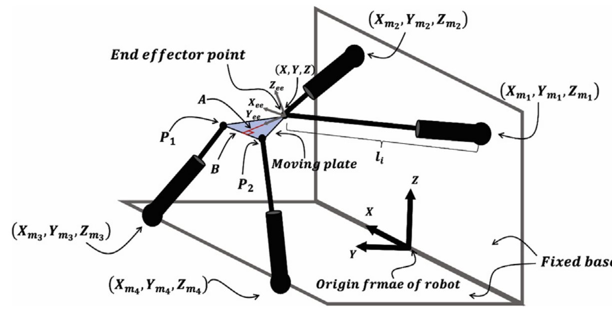


**Figure 5** Mechanism of EET guiding robot.

## 2.5. Robot simulation and workspace determination

The kinematic model of the EET guiding robot is determined in the previous section. In this section, the EET guiding robot is simulated by using MATLAB programming. An algorithm is developed based on the estimated kinematic models of equation (2) and equation (4). This algorithm simulates the EET guiding robot for workspace and dimensional observation as shown in Fig. 6a. Workspace and dimension of the guided robot are optimized to fit with the size of EET workspace. Workspace of the EET guiding robot is represented in 2D-plane with 30 $\times$ 30 mm length and 2 rotation angles range from $-15$ to 15°. The model of the EET guiding robot is achieved on CAD programming as shown in Fig. 6b.

# 3. EET cadaveric experimental setup

Bi-nasal endoscopic transsphenoid surgery was carried out on 70 soft adult cadavers without any prior history of head trauma or craniofacial surgery. The cadavers were dissected following the initial autopsy examination and approval of the Department of Anatomy, Faculty of Science, Mahidol University. Each cadaver was used for 2 experiments: left side and right side separately.

Polaris Vicra, optical tracking system from Northern Digital Inc. is used to detect and record positions and orientations of a surgical tool during the EET surgery on cadaveric cases. Two markers were used in the experiments; to attach with the surgical tool to represent the

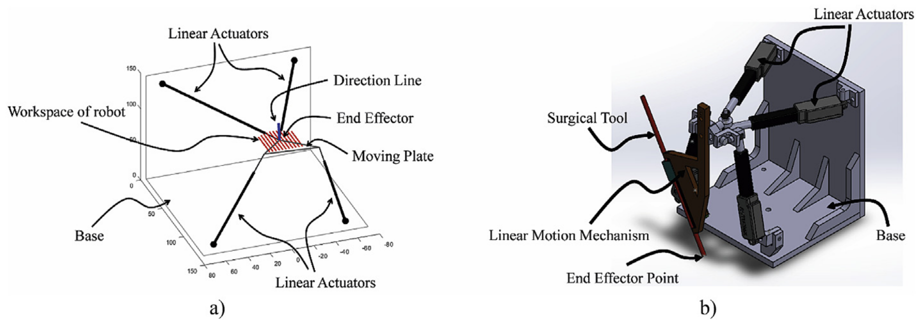


**Figure 6** Simulation of the EET guiding robot with workspace determination.

frame as illustrated in Fig. 7, and another marker attach with a tripod as reference coordinate. The optical tracking system defines surgical tool tip from tool tip calibration method which is Polaris Vicra's toolbox.

The optical tracking system recorded the movement of the tooltip with a maximum of 20 Hz frequency and 0.5 mm resolution. Tracking system recorded the surgical tool motion from the entry point of nostril towards the sphenoid sinus. The recorded data consisted of 6 variables; X-Y-Z positions (3 variables) and rotation angles around the X-Y-Z axis (3 variables). Fig. 8 shows the EET experiments on cadavers, 2 markers on the cadaver's head and surgical tool and NDI camera holder near the bed.

The recorded data was referenced on the NDI camera as homogeneous transformation matrices of ${}^{Camera}H_{Marker_2}$ and ${}^{Camera}H_{Marker_1}$ as shown in Fig. 7b). ${}^{Cadaver}H_{Tip}$ was estimated by using a mathematical method as represented in equation (5). ${}^{Cadaver}H_{Tip}$ represented the position and orientation of surgical tool tip on cadaver's origin frame. ${}^{Cadaver}H_{Tip}$ showed the preliminary result of the experiments.

$$
{}^{Cadaver}H_{Tip} = {}^{Camera}H^{-1}_{Marker_2} \cdot {}^{Marker_2}H^{-1}_{Cadaver} \cdot {}^{Camera}H_{Marker_1} \cdot {}^{Marker_1}H_{Tip} \tag{5}
$$

## 4. Results

### 4.1. Preliminary results

Fig. 9a depicts the preliminary result in cloud positions; red point indicates the position of the surgical tool tip. During the experiments, surgical tool insertion is initiated at an entry point of the nostril and terminates at the sphenoid sinus and earns around 800 points per experiment as shown in Fig. 9a. Fig. 9b shows the shape of cloud positions by a dotted line and the cloud collection shape is identical to a cylindrical tube with narrow part at middle area. For understanding, the cloud position was mapped on the head's anatomy as shown in Fig. 9c.

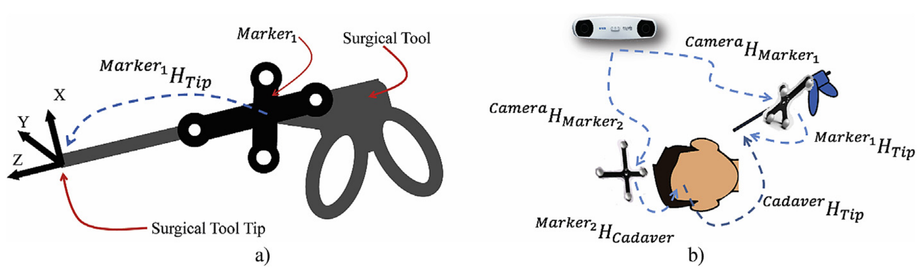


**Figure 7** a) Surgical tool and marker and b) Transformation matrices of the experiments.

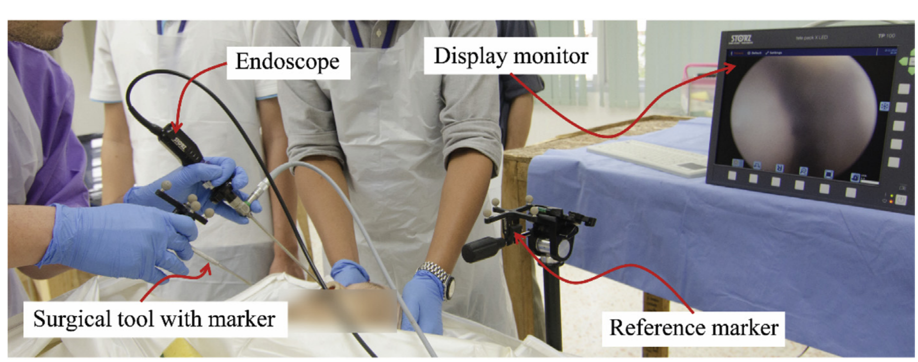


**Figure 8** EET experiment on cadaver.

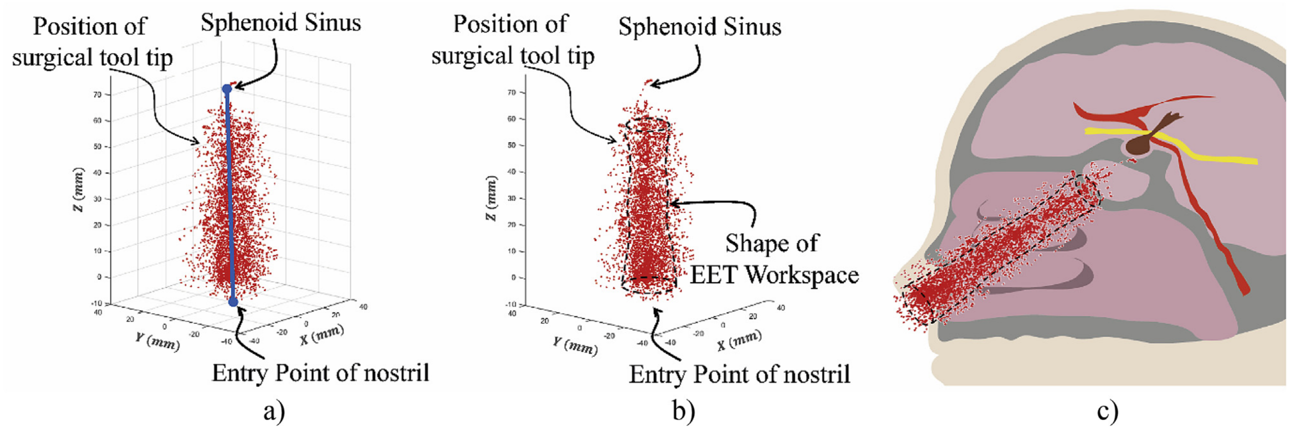


**Figure 9** a) Cloud position of preliminary Result, b) Preliminary Result with Shape of EET workspace and c) Preliminary result overlay on head anatomy for understanding.

### 4.2. EET workspace

As illustrated in Table 1, shape, dimension and volume of cloud position from preliminary result has been used to determine EET workspace. Results of EET workspace are present in Table 1. The statistical data shows the variation of EET workspace from 140 samples (n = 140). The table shows volume, smallest diameter and length of EET workspace from both sides i.e. left and right side. The table further shows statistical data of minimum, maximum, average and standard deviation values for all the three parameters. Shape of EET workspace is assumed as cylinder as shown in Fig. 9b.

### 4.3. EET pathway/motion

Cloud position data is analyzed by voxelization method as described in chapter 2. Fig. 10 shows result of EET pathway. The pathway starts from the entry point of nostril until the endpoint at anterior sphenoid bone. A line on the figure shows the center line of EET workspace between the entry point of the nostril and the sphenoid bone. Arrows represents voxels with high PDF value (high density of cloud point position); size of the arrows represent high PDF value (density of cloud point at each position) and direction of arrows represent high PDF value of cloud point direction.

**Table 1** EET workspace analysis from cloud position data.

| | | Statistical Data | | | |
|---|---|---|---|---|---|
| | | Minimum | Maximum | Average | Standard Deviation |
| Volume ($cm^3$) | Left | 7.73 | 26.86 | 16.16 | 5.92 |
| | Right | 5.61 | 28.87 | 15.78 | 6.2 |
| | All | 5.61 | 28.87 | 15.97 | 6.02 |
| Diameter ($mm$) | Left | 14.28 | 25.89 | 19.32 | 3.23 |
| | Right | 13.28 | 27.26 | 18.84 | 3.46 |
| | All | 13.28 | 27.26 | 19.08 | 3.32 |
| Length ($mm$) | Left | 36.01 | 70.46 | 53.55 | 8.39 |
| | Right | 40.5 | 70 | 54.24 | 5.91 |
| | All | 36.01 | 70.46 | 53.9 | 7.2 |

## 5. Discussion

Initially, the cloud position was collected through the routine surgeries performed via EET procedure. The data was analyzed and tested at 70 soft cadavers. The results depicted a sharp reduction in time required to conduct the surgery. This system is established on the results obtained in Table 1, where the experiment was conducted on both sides of the nostrils. The data obtained via this experiment shows the average values for length, diameter and volume. Therefore, a standard receptacle is designed so that it is adjustable in any workspace. The values obtained for length, diameter and volume were: 7.2 3.32 and 6.02 S.D. respectively.

Moreover, the EET pathway as in Fig. 10 shows the high density region, which allows the space for surgical tool insertion as show in Fig. 10b. The volume was called as safe space that is allows the surgical to reach the sphenoid sinus with a straight line insertion and is a substantial information for robot designing. Consequently, an EET robot guided procedure can be performed as a single time insertion. Furthermore, this study also shows that with the addition of robot guided receptacle the time period to conduct EET procedure has reduced significantly. As this is an immensely sensitive surgery, so the convenient and efficient workspace along with a stable pathway must be provide to the surgeon.

However, limitation to the result emanates from the use of soft cadavers, which are preserved under a temperature of 0 °C without the use of formalin. In such cadavers, the workspace is a little wider and the soft tissue shrinks due to being non-epinephrine, and the case is quite contrast in a living person. Therefore, their might be certain variations in comparison with real-life surgeries via EET guided robot systems. Furthermore, this study is only conducted on cadavers available were from Southeast Asia which might variate with cadavers available from other continents due to variable size and skin type of the nostrils and the nasal cavity.

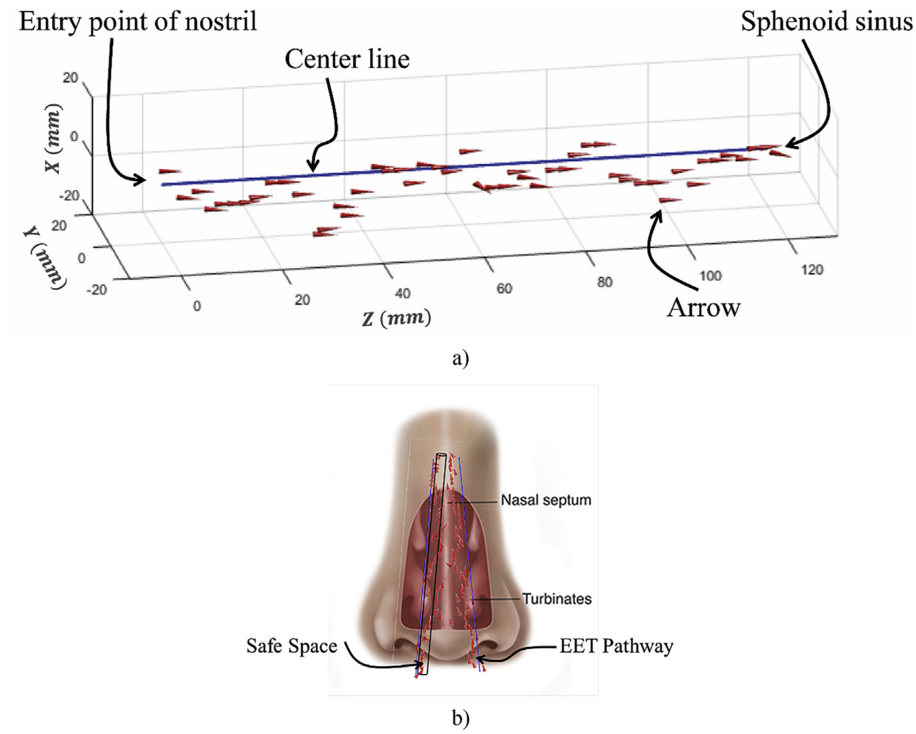


**Figure 10** a) Example of EET pathway and b) EET pathway on nose anatomy.

## 6. Conclusion

This article describes a study that is conducted on the EET surgical procedure, which examined the workspace and pathway of EET surgery. The procedure was explored on real EET surgeries and was experimented on cadavers. The experiments were performed on 70 cadavers, during which, an analysis of the EET workspace and the EET pathway were conducted through the cloud positions of the surgical tool tip. The result from the EET pathway was noteworthy, as the surgical tool was able to reach sphenoid sinus by a single time insertion. Through the dimensions of the EET workspace and attributes of the EET pathway, the design specifications of the EET guided robot could be determined. Thus, the EET robot was designed to guide a surgeon approaching the sinus. Also, the kinematic models of the EET guided robot was established. Regarding the article, the operations of the EET guided robot are delineated, as well as the leads and detriments of the EET robotic system are highlighted.

## Ethical approval

Cadaveric based experiments were conducted and an Ethical approval statement is enclosed as an electronic supplementary material.

## Disclosure of conflict of interest

The authors declare that they have no competing interests.

## Acknowledgements

This research is financially supported by National Research University Funds through Mahidol University. The authors would like to thank Clinical Anatomy and Research Education Laboratory, (CARE LAB) for collaboration of cadaver experiments. And also Ramathibodi hospital for EET surgeries observation. Moreover, we would like to thank BART LAB members for technical support.

## References

1. Christian E, Harris B, Wrobel B, Zada G. Endoscopic endonasal transsphenoidal surgery: implementation of an operative and perioperative checklist. *Neurosurg Focus*. 2014;37:E1.
2. Solari D, Villa A, Angelis M, Esposito F, Cavallo LM, Cappabianca P. Anatomy and surgery of the endoscopic endonasal approach to the skull base. Translational Medicine @ UniSa. 2012;2:36—46.
3. Zhang X, Fei Z, Zhang W, et al. Endoscopic endonasal transsphenoidal surgery for invasive pituitary adenoma. *J Clin Neurosci*. 2008;15:241—245.
4. Autorino R, Yakoubi R, White WM, et al. Natural orifice transluminal endoscopic surgery (NOTES): where are we going? A bibliometric assessment. *BJU Int*. 2013;111:11—16.
5. Bergman S, Melvin WS. Natural orifice translumenal endoscopic surgery. *Surg Clin North Am*. 2008;88:1131—1148.
6. Kassam AB, Prevedello DM, Carrau RL, et al. Endoscopic endonasal skull base surgery: analysis of complications in the authors' initial 800 patients. *J Neurosurg*. 2011;114:1544—1568.
7. Jho HD, Carrau RL. Endoscopic endonasal transsphenoidal surgery: experience with 50 patients. *J Neurosurg*. 1997;87:44—51.
8. Molitch ME. Diagnosis and treatment of pituitary adenomas: a review. *J Am Med Assoc*. 2017;317:516—524.

9. Garcia-Garrigos E, Arena-Jimenez J, Monjas-Canovas I, et al. Transsphenoidal approach in endoscopic endonasal surgery for skull base lesions: what radiologists and surgeons need to know. *Radiographics*. 2015;35:1170—1185.
10. Gondim JA, Almeida JP, Albuquerque LA, et al. Endoscopic endonasal approach for pituitary adenoma: surgical complications in 301 patients. *Pituitary*. 2011;14:174—183.
11. Berker M, Hazer DB, Yucel T, et al. Complications of endoscopic surgery of the pituitary adenomas: analysis of 570 patients and review of the literature. *Pituitary*. 2012;15:288—300.
12. Wang F, Zhou T, Wei S, et al. Endoscopic endonasal transsphenoidal surgery of 1,166 pituitary adenomas. *Surg Endosc*. 2015;29:1270—1280.
13. Abe LI, Iwao Y, Gotoh T, et al. High-speed point cloud matching algorithm for medical volume images using 3D Voronoi diagram. In: *2014 7th International Conference on Biomedical Engineering and Informatics*. 2014:205—210. https://doi.org/10.1109/BMEI.2014.7002771.
14. Suthakorn J, Chirikjian GS. A new inverse kinematics algorithm for binary manipulators with many actuators. *Adv Robot*. 2001;15:225—244.
15. Kazanzides P, Fichtinger G, Hager GD, Okamura AM, Whitcomb LL, Taylor RH. Surgical and interventional robotics: core concepts. *Technol Des*. 2010;15:122—130.
16. Fichtinger G, Kazanzides P, Okamura AM, Hager GD, Whitcomb LL, Taylor RH. Surgical and interventional robotics: Part II: surgical CAD-CAM systems. *IEEE Robot Autom Mag*. 2008;15:94—102.
17. Hager GD, Okamura AM, Kazanzides P, Whitcomb LL, Fichtinger G, Taylor RH. Surgical and interventional robotics: Part III: surgical assistance systems. *IEEE Robot Autom Mag*. 2008;15:84—93.
18. Gao F, Li W, Zhao X, Jin Z, Zhao H. New kinematic structures for 2-, 3-, 4-, and 5-DOF parallel manipulator designs. *Mech Mach Theor*. 2002;37:1395—1411.
19. Cheung JWF, Hung YS. Modelling and control of a 2-DOF planar parallel manipulator for semiconductor packaging systems. In: *Proceedings, 2005 IEEE/ASME International Conference on Advanced Intelligent Mechatronics*. 2005:717—722. https://doi.org/10.1109/AIM.2005.1511067.
20. Wu J, Wang J, Li T, Wang L. Dynamic analysis of the 2-DOF planar parallel manipulator of a heavy duty hybrid machine tool. *Int J Adv Manuf Technol*. 2007;34:413—420.
21. Figielski A, Bonev IA, Bigras P. *Towards Development of a 2-DOF Planar Parallel Robot with Optimal Workspace Use*. 2007:1562—1566.
22. Joubair A, Slamani M, Bonev IA. Kinematic calibration of a five-bar planar parallel robot using all working modes. *Robot Comput Integrated Manuf*. 2013;29:15—25.
23. Duan X, Yang Y, Cheng B. Modeling and analysis of a 2-DOF spherical parallel manipulator. *Sensors (Basel, Switzerland)*. 2016;16.
24. Liu H, Mei J, Zhao X, Huang T, Chetwynd DG. Inverse dynamics and servomotor parameter estimation of a 2-DOF spherical parallel mechanism. *Sci China Ser E Technol Sci*. 2008;51:288—301.